Int. J. Solids Structures Vol. 27, No. 14, pp. 1789–1807, 1991
Printed in Great Britain

0020–7683/91 $3.00 + .00
© 1991 Pergamon Press plc

INFLUENCE OF FRICTIONAL SHEAR STRESSES ON BIFURCATION IN LAYERED SOLIDS

PAUL S. STEIF
Department of Mechanical Engineering, Carnegie-Mellon University, Pittsburgh, PA 15213-3890, U.S.A.

(*Received* 7 *January* 1990; *in revised form* 1 *August* 1990)

Abstract—The effects of shearing on the emergence of bifurcation modes during the rolling of clad metals are studied. Previous studies of bifurcation modes in layered solids assumed that rolling could be modeled as a simple, homogeneous compression, with zero shear stress acting parallel to the layers. This clearly ignores friction which is necessarily present between the sheets and the rolls. In this paper, two new prebifurcation states, each reminiscent of a different type of shearing that occurs in rolled clad metals, are considered; their tendencies to provoke bifurcation modes are contrasted with previous predictions based on frictionless compression. As the governing differential equation for incremental deformations is substantially more complex than before, a numerical approach is devised to compute the bifurcation strains. The results of this approach, which are shown to be extremely accurate by comparison with previously obtained results, indicate that approximating rolling as a homogeneous, frictionless compression may lead to substantial errors.

1. INTRODUCTION

During the process of roll-bonding clad metals (illustrated schematically in Fig. 1), and during the rolling of already bonded clads, there occasionally occurs a spatially periodic variation in the thickness of individual layers. While this variation may be so slight as to be unnoticeable, it can also be so extreme as to cause an inner layer to break through the cladding. The periodic stripes of core material penetrating the cladding are sometimes referred to as tiger bands. In Fig. 2 we show this layer thickness variation, as observed by Semiatin and Piehler (1979), in an already bonded stainless steel clad aluminum subjected to rolling. This phenomenon, which can be highly detrimental to the final properties of the clad, is still poorly understood. The ability to predict the onset and development of layer thickness variations would have a positive impact on the processing of clad metals.

Recently, a bifurcation model for the appearance of tiger bands during rolling has been presented by the author (Steif, 1987, 1990). In Steif (1987), rolling was idealized as a homogeneous, plane strain compression, and the strain at which a periodic deformation pattern akin to tiger banding can exist was calculated. With a view to understanding tiger banding during *roll bonding*, Steif (1990) reconsidered this problem, but relaxed the condition of tangential velocity continuity between the layers. This reflects the fact that the various sheets entering the bonding mill are not bonded to one another; the ease of slippage would depend on the inter-layer friction which was taken to be zero. The reductions at which tiger banding is possible were found to be substantially lower when tangential slippage is permitted.

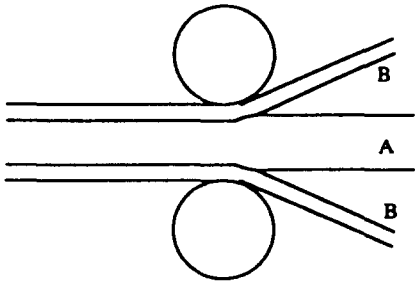

Fig. 1. Schematic of roll bonding.

The present paper is in the spirit of Steif (1990) in that it attempts to test the sensitivity of the predicted bifurcation strains to certain idealizations which may be at odds with reality. In particular, we will examine how the presence of shear stresses parallel to the interface affects predictions for the onset of tiger banding. Both previous attempts by the author to model the emergence of thickness variations assumed that rolling can be viewed as a plane strain compression which is imposed by rigid, frictionless platens. This simple homogeneous prebifurcation state is an idealization for two reasons. First, when the sheets are not symmetric about the center line between the rolls, or when the rolls are driven at different speeds, there are likely to be shear stresses acting parallel to the interface, in addition to the compression and tension that have been considered thus far. In order to simulate this shear stress, we will consider a prebifurcation state which has a homogeneous shear stress superposed on the simple compression.

Secondly, even when bonding a symmetric clad, the friction at the rolls induces shear stresses; these stresses are anti-symmetric about the center line, attaining a maximum value at the rolls. Below, we will present a prebifurcation stress state which reflects the inhomogeneous shearing to be found when rolling a symmetric clad. To appreciate this stress state, some historical background is necessary. von Karman's (1925) pioneering one-dimensional analysis of sheet rolling pointed out the significant role played by friction when the rolls draw a sheet in at the entrance and then resist the sheet's leaving at the exit. However, the earliest rolling analyses assumed that the deformation is homogeneous in each cross-section along the roll arc (the so-called slab method), and that the yielding is independent of the shear stress. The severely inhomogeneous state of strain that exists in reality is illustrated most vividly in a classic paper by Orowan (1943), in which, among other things, he presents a photograph of a slab of plasticine, containing alternating dark and light layers, which was rolled with high friction.

While Orowan (1943) did not present a rolling analysis which accounts for the highly inhomogeneous strain state that he observed in the plasticine, he did suggest a stress state which is somewhat more realistic than the uniform deformation of the slab method. Orowan appealed to Prandtl's (1923) plane strain solution for a very long, thin, perfectly plastic slab which is compressed between two rigid, *rough* platens (see Fig. 3a). In Prandtl's solution, which is valid away from the central part of the slab where the material would remain elastic, the shear stress varies linearly across the thickness and reaches the shear flow stress at the platens. This allows relative motion between the slab and the rough platen, as the curved slip lines are tangential to the slab–platen interface. Orowan (1943) suggested that the shear stresses acting on a rolled sheet are essentially the same as those acting on the compressed slab (compare Figs 3a and 3b), except for the curvature associated with the rolls. Below, we will show how the Prandtl–Orowan solution can be extended to a symmetrically layered solid. This new solution, which is only approximate for a hardening material, will constitute the prebifurcation field which reflects the shearing which is inherent in the rolling process.

In Section 2, we set forth the prebifurcation fields to be considered, including a bimaterial version of Prandtl's compressed slab solution. Section 3 contains a derivation of the equations for incremental deformations at finite strain which are appropriate to the present problem featuring a particular class of inhomogeneous prebifurcation states. In Section 4, the bifurcation problem is posed and the forms of the eigenmodes are discussed. A highly accurate numerical scheme for determining the eigenstrains (reductions at which tiger banding is possible) is presented in Section 5. The results are presented and discussed in Section 6, followed by a summary and conclusions in Section 7.

2. PREBIFURCATION STATES

In this section we present the two prebifurcation states to be considered in the study of the effect of shearing on the emergence of tiger bands. The first state is intended to capture the shearing which is associated with rolling an unsymmetric set of layers, or which would arise from driving the rolls at different speeds. It consists of the homogeneous compressive stress normal to the sheets considered in previous work, on which we superpose

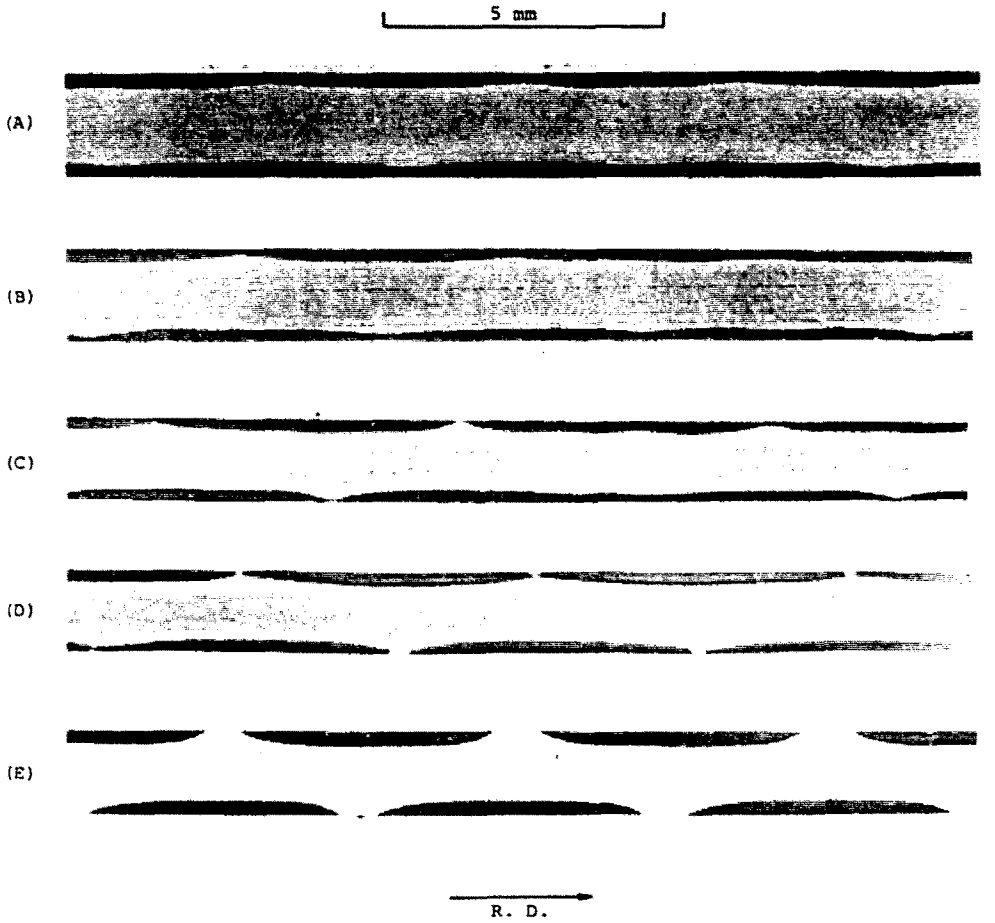

Fig. 2. Layer thickness variation leading to tiger banding in a rolled stainless steel clad aluminum.

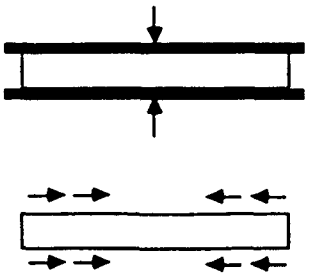

Fig. 3a. Prandtl problem of a thin slab compressed between rough platens.

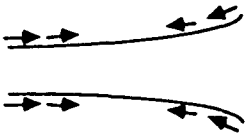

Fig. 3b. Shear stresses during rolling.

a uniform shear stress. The finite strain solution for combined compression and shear is now presented for a layered solid in which the individual materials are incompressible, and are characterized by an isotropic, hyperelastic, J_2-deformation theory of plasticity (Hutchinson and Neale, 1978). In Section 3, this choice of material law will be justified.

A three-layered solid to be subjected to extension and shear is shown schematically in Fig. 4. For an incompressible material deforming in plane strain, three parameters define the kinematics of this piece-wise constant deformation: ε, the logarithmic strain in the horizontal direction (equal to the same value in all layers); γ_A, the shear strain angle in A; and γ_B, the shear strain angle in B. This combination of strains ensures compatibility of deformations, and would be appropriate for any stacking sequence involving layers of two materials A and B. Note that the three parameters ε, γ_A and γ_B are not independent. In particular, we imagine the loading to be described by ε and γ_A; γ_B is determined by the condition that the shear stress is continuous across the interface.

For a solid subjected to an extension ε and a shear γ, the principal stretches are given by

$$\lambda_1 = \cosh 2\varepsilon + \tfrac{1}{2}\gamma^2 + \sqrt{\sinh^2 2\varepsilon + \gamma^2 \cosh 2\varepsilon + \tfrac{1}{4}\gamma^4} \tag{1a}$$

$$\lambda_2 = \cosh 2\varepsilon + \tfrac{1}{2}\gamma^2 - \sqrt{\sinh^2 2\varepsilon + \gamma^2 \cosh 2\varepsilon + \tfrac{1}{4}\gamma^4}. \tag{1b}$$

These stretches preserve incompressibility in that $\lambda_1\lambda_2 = 1$. From the stretches, one can find the logarithmic strains

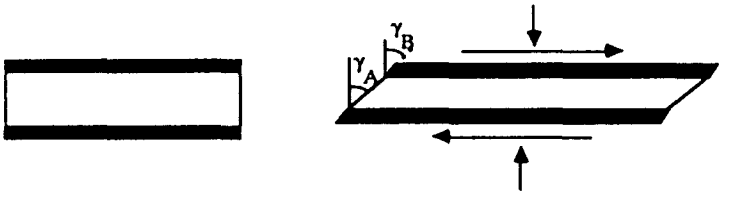

Fig. 4. Symmetrically clad, three-layer solid subjected to extension and shearing.

$$\varepsilon_1 = \ln \lambda_1 \quad \varepsilon_2 = \ln \lambda_2. \tag{2a, b}$$

The J_2-deformation theory of plasticity takes the principal Cauchy stress difference $\sigma_1 - \sigma_2$ to be related to the principal strain difference according to

$$\sigma_1 - \sigma_2 = \tfrac{2}{3} E_s (\varepsilon_1 - \varepsilon_2) \tag{3}$$

where E_s is the secant modulus.

In terms of ε and γ, the principal directions are at angles θ^* and $\theta^* + \pi/2$ from the x_1 axis, where θ^* satisfies

$$\sin 2\theta^* = \frac{\gamma \, e^{-\varepsilon}}{\sqrt{\sinh^2 2\varepsilon + \gamma^2 \cosh 2\varepsilon + \frac{1}{4}\gamma^4}}. \tag{4}$$

By combining (1)–(4) and the usual transformation formulae for stress components, one can find the shear stress component σ_{12}, which must be continuous across the interface. Equating the expressions for σ_{12} in A and B leads to a single equation for γ_B, in terms of the strains ε and γ_A, and material parameters in A and B (which determine E_s in A and B). The remaining quantities required for the bifurcation analysis can be readily derived.

Now, we present the prebifurcation stress state which is intended to mimic the shearing which is inherent in the rolling process, even in ideally symmetric rolling. We consider the problem of a symmetric laminate of three sheets, which are compressed by rough, rigid platens (see Fig. 5). For now, we assume that all sheets are rigid, perfectly plastic; the outer sheets have a plane strain tensile yield stress σ_B, and the inner sheet has a plane strain tensile yield stress σ_A. Of interest are solutions in which all layers are deforming, and for which the deviatoric stresses are independent of the coordinate x_1. Our solution to this problem is motivated by Prandtl's (1923) solution to the single-layer problem (Fig. 3a) which is given by

$$\sigma_{11} = -\left(c + \frac{x_1 \sigma_Y}{2b}\right) + \sigma_Y \sqrt{1 - \left(\frac{x_2}{b}\right)^2} \tag{5a}$$

$$\sigma_{22} = -\left(c + \frac{x_1 \sigma_Y}{2b}\right) \tag{5b}$$

$$\sigma_{12} = \frac{x_2 \sigma_Y}{2b} \tag{5c}$$

where σ_Y is the yield stress of the layer, c is any constant, and the layer has a thickness $2b$. This solution presumes that the platens are sufficiently rough to sustain a shear stress equal to the shear yield stress of the material $\frac{1}{2}\sigma_Y$. The curved slip lines are tangential to the platen–metal interface; thus, relative motion can occur along this interface. Note that this solution is valid in the left portion of the sheet, away from the center (where the layer would not be yielding plastically) and away from the ends (where end-effects will be significant).

Orowan (1943) took the Prandtl (1923) solution and used it to include the effect of the shear stress on the yield condition at some point along the roll arc. Let σ denote the average tensile stress σ_{11} at a given cross-section, and let p denote the roll pressure $(-\sigma_{22})$. Instead of the equation

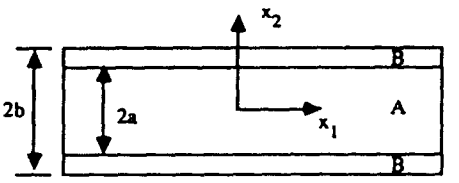

Fig. 5. Definition of coordinates and dimensions in symmetrically clad, three-layer solid.

$$\sigma+p=\sigma_Y \tag{6}$$

which is commonly used in rolling analyses, and which is a reasonable approximation for low shear stresses at the rolls. Orowan proposed the following equation:

$$\sigma+p=\frac{\pi}{4}\sigma_Y. \tag{7}$$

This was obtained from the Prandtl solution by integrating over the cross-section. Clearly, this approximation is most appropriate when the roll friction is very high.

For moderate levels of friction, Orowan utilized the stress distribution

$$\sigma_{11}=-\left(c+\frac{x_1\tau_p}{b}\right)+\sigma_Y\sqrt{1-\left(\frac{2\tau_p x_2}{\sigma_Y b}\right)^2} \tag{8a}$$

$$\sigma_{22}=-\left(c+\frac{x_1\tau_p}{b}\right) \tag{8b}$$

$$\sigma_{12}=\frac{x_2\tau_p}{b} \tag{8c}$$

where he interpreted the spatially constant shear stress at the platen–metal interface, τ_p, to be equal to a Coulomb friction coefficient times the pressure. From this, one finds a yield condition which is somewhere between (6) and (7), depending on where τ_p lies along the interval $0 \leqslant \tau_p \leqslant \frac{1}{2}\sigma_Y$. Orowan immediately recognized that this solution is not strictly valid over any finite extent of the compressed strip, as the interfacial shear stress is constant, while the pressure varies linearly with x_1. Nevertheless, given all the approximations in these one-dimensional theories for rolling, the distribution seems to be a useful approximation.

It is relatively straightforward to take the Prandtl and Orowan solutions for the single-layer problem and generate the following one-parameter family of solutions to the three-layer problem:

in A:

$$\sigma_{11}=-\left(c+\frac{x_1 m\sigma_B}{2b}\right)+\sigma_A\sqrt{1-\left(\frac{m\sigma_B x_2}{\sigma_A b}\right)^2} \tag{9a}$$

$$\sigma_{22}=-\left(c+\frac{x_1 m\sigma_B}{2b}\right) \tag{9b}$$

$$\sigma_{12}=\frac{x_2 m\sigma_B}{2b} \tag{9c}$$

in B:

$$\sigma_{11}=-\left(c+\frac{x_1 m\sigma_B}{2b}\right)+\sigma_B\sqrt{1-\left(\frac{x_2}{b}\right)^2} \tag{9d}$$

$$\sigma_{22}=-\left(c+\frac{x_1 m\sigma_B}{2b}\right) \tag{9e}$$

$$\sigma_{12}=\frac{x_2 m\sigma_B}{2b} \tag{9f}$$

where the parameter m is a positive constant. These solutions satisfy the equilibrium equations and the yield condition in each of A and B, as well as continuity of traction at

the interfaces between the layers. In addition, one can show that the corresponding strain fields are derivable from velocities which are continuous at the interface. For $m = 1$, the shear stress in B at the platens is equal to the shear yield stress $\frac{1}{2}\sigma_B$, which allows B to slip relative to the rough, rigid platens. Note that when $m = 1$ and $\sigma_A = \sigma_B = \sigma_Y$, this solution reverts to the original Prandtl solution (5). An obvious feature of eqns (9), and one that is crucial to a reinterpretation introduced below, is that the Von Mises invariant is constant in each of A and B and equal, of course, to the respective yield strengths.

Introducing the family of solutions parameterized by m serves the same purpose as does Orowan's generalization of the Prandtl solution. The specific case of $m = 1$ corresponds to a shear stress in material B at the platen which is equal to the shear yield stress $\frac{1}{2}\sigma_B$; when the platens are insufficiently rough to sustain this shear stress, m will be less than 1. There is a second restriction on m, in addition to the obvious one of $m \leqslant 1$: the solution is valid only if $m < m^*$, where m^* is defined by

$$m^* = \frac{\sigma_A}{\sigma_B}\frac{b}{a}. \tag{10}$$

This value m^*, which can be greater than or less than one, corresponds to a shear stress at the A–B interface which is equal to the shear yield stress of A. Any higher value of m would violate yield in material A. When $m \leqslant m^* < 1$, the platens may be too rough to allow slippage of material B. We ignore this possibility and assume that the platen–metal interface is such that the stress state given by (9) is permitted to exist over the range $0 \leqslant m \leqslant m_{cr}$, where m_{cr} is the minimum of m^* and 1, and that layer B is allowed to slip relative to the platen at this level of shear stress.

The materials of interest to the bifurcation studies, however, are not perfectly plastic; the hardening rates in A and B are consistently found to be crucial parameters in bifurcation analyses. To make the necessary leap to hardening materials, we simply follow Orowan's approach to rolling by *reinterpreting* the stress fields in (9) as pertaining to hardening materials. Obviously, at a minimum, we must adopt a plasticity theory in which the yield stress is a function of the Von Mises invariant, such as J_2-deformation theory. Since, as was pointed out above, the Von Mises invariant is constant in each of A and B, the current level of the flow stress is constant in each of A and B. The flow stresses change, however, as the sheets are compressed; that is, σ_A and σ_B are functions of the remote loading (as detailed below), but at any instant they are spatially constant. Unfortunately, this is not a rigorous solution to the problem when the materials harden; while mechanical equilibrium is satisfied, the effective strain (analogous to the Von Mises invariant of the stresses) will not be constant spatially and is, thus, incompatible with the assumption of a yield stress that remains spatially constant.

Nevertheless, we will use this field as the prebifurcation state, and we justify its use by appealing to the major purpose of this investigation: to assess the sensitivity of predictions of tiger banding to deviations from the previously assumed prebifurcation state of homogeneous, frictionless compression. It is presumed that this bimaterial generalization of the Prandtl field, despite its approximate nature for hardening materials, will provide useful, qualitative insight into the sensitivity of bifurcation predictions to the shear stresses associated with the friction inherent in rolling. In employing this field, we are assuming that the proper level of shear stress is provided at the platen–metal interface, and that it is uniform in x_1.

3. FIELD EQUATIONS

In this section a brief review is given of the relevant field equations for solids deformed into the finite strain range. We introduce the nominal stress with components n_{ij}, and the Cauchy (true) stress σ_{ij}, where all components are taken with respect to a fixed Cartesian frame. As is typical in bifurcation analyses, the reference configuration is taken to coincide instantaneously with the current configuration. Then, the material time derivative of

the components is related by

$$\dot{n}_{ij} = \overset{\nabla}{\sigma}_{ij} + \tfrac{1}{2}[\sigma_{ik}v_{j,k} - \sigma_{ik}v_{k,j} - \sigma_{jk}v_{i,k} - \sigma_{jk}v_{k,i}] \tag{11}$$

where the summation convention on repeated indices is assumed, $(\ )_{,i}$ denotes a partial derivative with respect to the spatial variable x_i, $\dot{n}_{ij}$ is the material time derivative of n_{ij}, $\overset{\nabla}{\sigma}_{ij}$ denotes the (objective) Jaumann derivative of the Cauchy stress, and v_i are the velocity components. Below, it will be assumed that the strain-rates are related to the Jaumann rate of the Cauchy stress. Continuing mechanical equilibrium is readily expressed in terms of the nominal stress-rate by

$$\dot{n}_{ij,i} = 0. \tag{12}$$

We now specialize these equations to an incompressible solid deforming in the x_1–x_2 plane. Incompressibility implies that the velocities are derivable from a scalar stream function $\chi(x_1, x_2)$ according to

$$v_1 = \chi_{,2} \quad v_2 = -\chi_{,1}. \tag{13a, b}$$

Following Hill and Hutchinson (1975), we write the two relevant equilibrium equations in the following form which is useful for incompressible materials:

$$\tfrac{1}{2}(\dot{n}_{11} - \dot{n}_{22})_{,1} + \dot{n}_{21,2} = -\tfrac{1}{2}(\dot{n}_{11} + \dot{n}_{22})_{,1} \tag{14a}$$

$$\tfrac{1}{2}(\dot{n}_{11} - \dot{n}_{22})_{,2} - \dot{n}_{12,1} = \tfrac{1}{2}(\dot{n}_{11} + \dot{n}_{22})_{,2}. \tag{14b}$$

At this point, we justify the constitutive law introduced in Section 2. First, as was explained above, a reinterpretation of the stress state (9) as pertaining to hardening materials requires the material law to be based on the Von Mises or J_2 invariant. In choosing J_2-deformation theory, we appeal to the long-standing appreciation that the particular choice of hardening rule has serious consequences for bifurcation predictions, such as buckling and necking (Hutchinson, 1974). In particular, a plasticity theory based on a smooth yield surface, which implies a stiff (elastic) response to non-proportional stress increments, consistently leads to very high predictions of bifurcation strains. On the other hand, when a deformation plasticity theory is used, or when the yield surface has a vertex, bifurcation predictions are lower and more reasonable. Consistent with this experience, therefore, we take the material to be described by J_2-deformation theory. This is convenient in that the limit of $m \to 0$ in (9) corresponds to a uniform, frictionless compression—the prebifurcation state previously studied (Steif, 1987, 1990); thus, this limiting case can readily provide a test of the numerical technique which is introduced in Section 5.

In the case of plane strain deformations, J_2-deformation theory connects the components of the Jaumann stress-rate to the strain-rates according to the relation

$$\overset{\nabla}{\sigma}_{ij} = \tfrac{2}{3}E_m\dot{\varepsilon}_{ij} - \frac{E_m - E_t}{3J_2}s_{ij}s_{kl}\dot{\varepsilon}_{kl} + \dot{p}\delta_{ij} \tag{15}$$

where δ_{ij} is the Kronecker delta, E_m is a modified secant modulus defined below, and $\dot{p}$ is the hydrostatic pressure-rate. The tangent modulus, E_t, depends on J_2, which is given by

$$J_2 = \tfrac{1}{2}s_{ij}s_{ij} \tag{16}$$

where the Cauchy stress deviator s_{ij}, is defined, as usual, by

$$s_{ij} = \sigma_{ij} - \tfrac{1}{3}\sigma_{kk}\delta_{ij}. \tag{17}$$

It is equivalent to viewing the moduli as functions of the effective stress, σ_e, which is

related to J_2 by $\sigma_e^2 = 3J_2$. Then, as is usually done in J_2-based plasticity theories, the tangent modulus for a given value of effective stress is obtained from the stress–strain curve measured in uniaxial tension.

In particular, we use (as in previous work) the hyperelastic J_2-deformation theory of Hutchinson and Neale (1978), in which case the modified secant modulus E_m is given by

$$E_m = \sqrt{3}\sigma_e \coth\left(\frac{\sqrt{3}\sigma_e}{E_s}\right) \tag{18}$$

where E_s is the actual secant modulus (defined from the uniaxial stress–strain curve).

By combining eqns (11)–(15), and the strain-rate velocity relation

$$\varepsilon_{ij} = \tfrac{1}{2}[v_{i,j} + v_{j,i}] \tag{19}$$

one can derive an extremely lengthy differential equation for the stream function χ. For our purposes, however, a special case of this very general equation suffices. Consideration of the two prebifurcation states presented in Section 2 indicates that, while the stresses may vary from point to point (they do in the bimaterial Prandtl–Orowan solution), the effective stress is always piece-wise constant; this implies that the secant and tangent moduli are piece-wise constant. Assuming, then, that the moduli are spatially constant, one can derive the following governing equation for the stream function χ:

$$\begin{aligned}
&[\tfrac{1}{3}E_m - \beta\sigma_{12}^2 + s_{11}]\chi_{,1111} + [\tfrac{2}{3}E_m + \beta(2\sigma_{12}^2 - 4s_{11}^2)]\chi_{,1122} + [\tfrac{1}{3}E_m - \beta\sigma_{12}^2 - s_{11}]\chi_{,2222} \\
&+ [4\beta\sigma_{12}s_{11} + 2\sigma_{12}]\chi_{,1112} + [-4\beta\sigma_{12}s_{11} + 2\sigma_{12}]\chi_{,2221} \\
&+ [2\beta(\sigma_{12}s_{11,2} + s_{11}\sigma_{12,2} - 2\sigma_{12}\sigma_{12,1}) - \sigma_{22,1}]\chi_{,111} \\
&+ [-2\beta(\sigma_{12}s_{11,1} + s_{11}\sigma_{12,1} + 2\sigma_{12}\sigma_{12,2}) - \sigma_{11,2}]\chi_{,222} \\
&+ [2\beta(3\sigma_{12}s_{11,1} + 3s_{11}\sigma_{12,1} + 2\sigma_{12}\sigma_{12,2} - 4s_{11,2}s_{11}) + 3\sigma_{12,1}]\chi_{,112} \\
&+ [-2\beta(3\sigma_{12}s_{11,2} + 3s_{11}\sigma_{12,2} - 2\sigma_{12}\sigma_{12,1} + 4s_{11,1}s_{11}) + 3\sigma_{12,2}]\chi_{,122} \\
&+ [2\beta(s_{11}\sigma_{12,12} + \sigma_{12,2}(\sigma_{12,2} + s_{11,1}) - \sigma_{12,1}(\sigma_{12,1} - s_{11,2}) - \sigma_{12}s_{11,12}) + \tfrac{1}{2}(\sigma_{11,22} - \sigma_{22,11})]\chi_{,11} \\
&+ [-2\beta(s_{11}\sigma_{12,12} + \sigma_{12,2}(\sigma_{12,2} + s_{11,1}) - \sigma_{12,1}(\sigma_{12,1} - s_{11,2}) - \sigma_{12}s_{11,12}) + \tfrac{1}{2}(\sigma_{22,11} - \sigma_{11,22})]\chi_{,22} \\
&+ [-2\beta(2s_{11}s_{11,12} + \sigma_{12}(s_{11,22} - s_{11,11}) + 2s_{11,2}(\sigma_{12,2} + s_{11,1}) \\
&+ 2s_{11,1}(s_{11,2} - \sigma_{12,1})) + 2\sigma_{12,22} + 2\sigma_{12,11}]\chi_{,12} = 0
\end{aligned} \tag{20}$$

where β is given by

$$\beta = \frac{E_m - E_t}{\sigma_e^2}.$$

Also of interest are the traction-rates $\dot{n}_{21}$ and $\dot{n}_{22,1}$, which are given by

$$\dot{n}_{21} = [-\tfrac{1}{3}E_m + \beta\sigma_{12}^2 + \tfrac{1}{2}(\sigma_{11} + \sigma_{22})]\chi_{,11} + [\tfrac{1}{3}E_m - \beta\sigma_{12}^2 - s_{11})]\chi_{,22} + [-2\beta\sigma_{12}s_{11} + \sigma_{12}]\chi_{,12} \tag{21a}$$

$$\begin{aligned}
-\dot{n}_{22,1} = {} & [2\beta\sigma_{12}s_{11} + \sigma_{12}]\chi_{,111} + [E_m + \beta(\sigma_{12}^2 - 4s_{11}^2) - \tfrac{1}{2}(\sigma_{11} + \sigma_{22})]\chi_{,112} \\
& + [-4\beta\sigma_{12}s_{11} + 2\sigma_{12}]\chi_{,122} + [\tfrac{1}{3}E_m - \beta\sigma_{12}^2 - s_{11}]\chi_{,222} \\
& + [2\beta(\sigma_{12}s_{11,1} + \sigma_{12,1}s_{11} + \sigma_{12,2}\sigma_{12}) + s_{11,2}]\chi_{,11} \\
& + [-2\beta(\sigma_{12}s_{11,1} + \sigma_{12,1}s_{11} + \sigma_{12,2}\sigma_{12}) - \tfrac{1}{2}(\sigma_{11} + \sigma_{22})_{,2}]\chi_{,22} \\
& + [-2\beta(\sigma_{12}s_{11,2} + \sigma_{12,2}s_{11} + 4s_{11}s_{11,1}) - (2\sigma_{11} + \sigma_{22})_{,1}]\chi_{,12}.
\end{aligned} \tag{21b}$$

(Note that the spatial derivative of $\dot{n}_{22}$ allows for the hydrostatic pressure-rate to be eliminated.)

In applying eqns (20) and (21) to an incremental bifurcation problem, the stresses and incremental moduli are those associated with the prebifurcation state. For the prebifurcation state consisting of a homogeneous shear stress superposed on the compression, the stresses are derivable from ε, γ_A and γ_B, as discussed above. From these stresses, one can compute the effective stress, and then the moduli from the uniaxial stress–strain curve. For the case of the modified Prandtl–Orowan solution, we view the prebifurcation state as parameterized by a *fictitious* uniform thickness strain. From this fictitious strain, given by $\varepsilon_{11} = -\varepsilon_{22} > 0$, $\varepsilon_{12} = 0$ (ε_{ij} equal in both layers), we compute the effective stress in each layer from the respective stress–strain curves, as well as the respective moduli. It is the effective stresses which are the quantities σ_A, and σ_B that appear in (9). This uniform thickness strain is fictitious since the modified Prandtl–Orowan solution is only approximate; as discussed in Section 2, the evolving strain cannot really be uniform. Nevertheless, this approximate, though perhaps reasonable, approach has the feature that it reduces precisely to the homogeneous, frictionless compression considered previously in the limit of $m \to 0$.

4. BIFURCATION MODES

In this section, we specify the two types of bifurcation modes which are of interest in connection with layer thickness variations. The anti-symmetric mode involves deformation of the core (material A) which is anti-symmetric about its centerline; that is

$$v_2(x_2) = v_2(-x_2). \tag{22}$$

The symmetric mode involves deformation of the core that is symmetric about its centerline; that is

$$v_2(x_2) = -v_2(-x_2). \tag{23}$$

Once either of these modes develops sufficiently, it can lead to periodic fracture of the cladding, as exhibited in the rolling of an already bonded stainless steel clad aluminum (depicted in Fig. 2). Previously, Steif (1987) predicted that the anti-symmetric mode (exhibited by the sample in Fig. 2) would emerge first (at a lower reduction) when the cladding is relatively thin and hard; the symmetric mode was predicted to emerge first when the core is relatively thin and hard. One issue of interest here is the effect of friction on the selection of bifurcation mode.

Given this decomposition into symmetric and anti-symmetric modes, we can restrict the field equations to the domain $0 < x_2 < b$, though we need to impose the boundary conditions

$$\chi_{,2}(x_1, 0) = \chi_{,222}(x_1, 0) = 0 \quad \text{(anti-symmetric mode)} \tag{24a}$$

$$\chi(x_1, 0) = \chi_{,22}(x_1, 0) = 0 \quad \text{(symmetric mode)}. \tag{24b}$$

We search for periodic eigenmodes which take the form

$$\chi(x_1, x_2) = f^A(x_2) \sin \omega x_1 + g^A(x_2) \cos \omega x_1 \tag{25a}$$

in A, and

$$\chi(x_1, x_2) = f^B(x_2) \sin \omega x_1 + g^B(x_2) \cos \omega x_1 \tag{25b}$$

in B, where $2\pi/\omega$ is the wavelength of the mode. Inserting the forms (25) into the field eqn

(20), and collecting terms proportional to $\sin \omega x_1$ and $\cos \omega x_1$, one obtains two coupled, fourth-order, ordinary differential equations for $f(x_2)$ and $g(x_2)$, which we write symbolically in the form

$$\mathscr{L}_s\{f, g\} = 0 \tag{26a}$$

$$\mathscr{L}_c\{f, g\} = 0. \tag{26b}$$

Previously, when rolling was idealized as a homogeneous, frictionless compression, it was sufficient to search for eigenmodes proportional only to, say, $\sin \omega x_1$. The corresponding calculation for eigenmodes proportional to $\cos \omega x_1$ would yield identical results. These modes become coupled [as can be seen from (20)], once there is shearing.

It may not be readily apparent that eigenmodes can be found in the separable form (25); why should the ordinary differential equations (26) be independent of x_1? Whether they are independent of x_1 is clearly tied to the form of the prebifurcation states. For the prebifurcation state consisting of a homogeneous shear stress superposed on the homogeneous compression, all field quantities are piece-wise constant; in particular they are independent of x_1. On the other hand, the stresses in the bimaterial Prandtl–Orowan solution do vary spatially. Notice, however, that the deviatoric stresses (and the moduli) are independent of x_1 and that the hydrostatic pressure varies linearly with x_1. Together, these imply that (26) will be independent of x_1.

In addition to satisfying (26), the eigenmodes must satisfy various boundary conditions. In particular, (24) imply the following two conditions on each of $f(x_2)$ and $g(x_2)$:

$$f'(0) = g'(0) = f'''(0) = g'''(0) = 0 \quad \text{(anti-symmetric mode)} \tag{27a}$$

$$f'(0) = g'(0) = f'''(0) = g'''(0) = 0 \quad \text{(symmetric mode)} \tag{27b}$$

where $(\,)'$ denotes a derivative with respect to x_2.

At the rigid platen ($x_2 = h$), the eigenmodes are required to satisfy zero normal velocity and zero shear traction-rate. While these boundary conditions are perfectly consistent with the previous model of rolling as a homogeneous compression induced by frictionless platens, the assumption of a vanishing shear traction-rate is less satisfying here when the prebifurcation field itself features non-zero shear stresses at the platen–metal interface. In reality, one expects there to be some change in the shear stress as incremental interfacial slippage occurs. Though this shear traction-rate is neglected at present, its effect probably should be investigated in the future.

Finally, the eigenmodes must satisfy certain continuity conditions at the interface $x_2 = a$. This includes continuity of traction-rate, as well as continuity of velocities. Although interfacial slippage—a discontinuity in the tangential velocity component—is not permitted here, it is readily included, as it was in Steif (1990). Two pairs of velocity continuity conditions, one corresponding to $\sin \omega x_1$, and one corresponding to $\cos \omega x_1$, are obtained from (13). Similarly, from the expressions for traction-rates given in (21), one can obtain two pairs of traction-rate continuity conditions.

5. NUMERICAL APPROACH TO BIFURCATION CALCULATION

The numerical approach taken to solving the class of bifurcation problems outlined above is perhaps best explained by contrast to the primarily analytic approach taken in past studies of layer bifurcation problems. In previous bifurcation studies (Steif, 1987, 1990), it was possible to find closed form solutions to the governing homogeneous, fourth-order differential equation for $f(x_2)$, in each of A and B, in terms of four simple functions. For example $f^A(x_2)$ could be written in the form

$$f^A(x_2) = c_1 f_1^A(x_2) + c_2 f_2^A(x_2) + c_3 f_3^A(x_2) + c_4 f_4^A(x_2) \tag{28}$$

where the functions $f_j^A(x_2)$ $(j = 1, \ldots, 4)$ are simple functions (combinations of trig-

onometric and hyperbolic functions), and c_j are constant coefficients. Identical forms can be found for the functions in B. Using the homogeneous boundary conditions at $x_2 = 0$ and $x_2 = b$, one can immediately eliminate half of the undetermined coefficients. Imposing the homogeneous continuity conditions at the interface leads to a set of four homogeneous linear equations for the remaining coefficients. The terms in the associated matrix depend nonlinearly on the applied strain and on the material parameters, but can be expressed in closed form. The bifurcation strain, which corresponds to the lowest strain at which there exists a non-trivial solution to the equations, was found by setting the determinant (which is calculated numerically) equal to zero. Here, with the governing differential equations substantially more complicated, obtaining closed form homogeneous solutions is prohibitive. Hence, a numerical approach was sought.

To state the previous approach in a different way: we considered the space of functions which satisfy the governing homogeneous differential equation, and we searched for functions in this space which satisfy the homogeneous boundary conditions at $x_2 = 0$ and $x_2 = b$, and the homogeneous continuity conditions at $x_2 = a$. The basis for this space of functions consists of the closed form, linearly independent, homogeneous solutions [i.e. $f_j^{\wedge}(x_2)$] to the governing differential equation. Any function within this space is identified, or parameterized, by the values of coefficients c_j. Though closed form solutions can no longer be found for the governing differential equations when the prebifurcation stress state is inhomogeneous, we can take advantage of the linearity (26) to establish a basis for the space of functions to be searched.

Let the basis function pairs $\begin{Bmatrix}\varphi_j^{\wedge}(x_2)\\ \psi_j^{\wedge}(x_2)\end{Bmatrix}$ $(j = 1, 2, \ldots, 8)$ be defined in the domain $0 < x_2 < a$ and satisfy the governing eqns (26), where $\varphi_j^{\wedge}(x_2)$ is associated with $f(x_2)$, and $\psi_j^{\wedge}(x_2)$ is associated with $g(x_2)$. Now, each of the function pairs satisfies different initial conditions at $x_2 = 0$; specifically,

$$
\begin{Bmatrix}\varphi_1^{\wedge}(0)\\ \psi_1^{\wedge}(0)\end{Bmatrix} = \begin{Bmatrix}1\\0\end{Bmatrix} \quad \begin{Bmatrix}\varphi_1^{\wedge'}(0)\\ \psi_1^{\wedge'}(0)\end{Bmatrix} = \begin{Bmatrix}\varphi_1^{\wedge''}(0)\\ \psi_1^{\wedge''}(0)\end{Bmatrix} = \begin{Bmatrix}\varphi_1^{\wedge'''}(0)\\ \psi_1^{\wedge'''}(0)\end{Bmatrix} = \begin{Bmatrix}0\\0\end{Bmatrix}
$$

$$
\begin{Bmatrix}\varphi_2^{\wedge}(0)\\ \psi_2^{\wedge}(0)\end{Bmatrix} = \begin{Bmatrix}1\\0\end{Bmatrix} \quad \begin{Bmatrix}\varphi_2^{\wedge'}(0)\\ \psi_2^{\wedge'}(0)\end{Bmatrix} = \begin{Bmatrix}\varphi_2^{\wedge''}(0)\\ \psi_2^{\wedge''}(0)\end{Bmatrix} = \begin{Bmatrix}\varphi_2^{\wedge'''}(0)\\ \psi_2^{\wedge'''}(0)\end{Bmatrix} = \begin{Bmatrix}0\\0\end{Bmatrix}
$$

$$
\begin{Bmatrix}\varphi_3^{\wedge}(0)\\ \psi_3^{\wedge}(0)\end{Bmatrix} = \begin{Bmatrix}1\\0\end{Bmatrix} \quad \begin{Bmatrix}\varphi_3^{\wedge'}(0)\\ \psi_3^{\wedge'}(0)\end{Bmatrix} = \begin{Bmatrix}\varphi_3^{\wedge''}(0)\\ \psi_3^{\wedge''}(0)\end{Bmatrix} = \begin{Bmatrix}\varphi_3^{\wedge'''}(0)\\ \psi_3^{\wedge'''}(0)\end{Bmatrix} = \begin{Bmatrix}0\\0\end{Bmatrix}
$$

$$
\begin{Bmatrix}\varphi_4^{\wedge}(0)\\ \psi_4^{\wedge}(0)\end{Bmatrix} = \begin{Bmatrix}1\\0\end{Bmatrix} \quad \begin{Bmatrix}\varphi_4^{\wedge'}(0)\\ \psi_4^{\wedge'}(0)\end{Bmatrix} = \begin{Bmatrix}\varphi_4^{\wedge''}(0)\\ \psi_4^{\wedge''}(0)\end{Bmatrix} = \begin{Bmatrix}\varphi_4^{\wedge'''}(0)\\ \psi_4^{\wedge'''}(0)\end{Bmatrix} = \begin{Bmatrix}0\\0\end{Bmatrix}
$$

$$
\begin{Bmatrix}\varphi_5^{\wedge}(0)\\ \psi_5^{\wedge}(0)\end{Bmatrix} = \begin{Bmatrix}0\\1\end{Bmatrix} \quad \begin{Bmatrix}\varphi_5^{\wedge'}(0)\\ \psi_5^{\wedge'}(0)\end{Bmatrix} = \begin{Bmatrix}\varphi_5^{\wedge''}(0)\\ \psi_5^{\wedge''}(0)\end{Bmatrix} = \begin{Bmatrix}\varphi_5^{\wedge'''}(0)\\ \psi_5^{\wedge'''}(0)\end{Bmatrix} = \begin{Bmatrix}0\\0\end{Bmatrix}
$$

$$
\begin{Bmatrix}\varphi_6^{\wedge}(0)\\ \psi_6^{\wedge}(0)\end{Bmatrix} = \begin{Bmatrix}0\\1\end{Bmatrix} \quad \begin{Bmatrix}\varphi_6^{\wedge'}(0)\\ \psi_6^{\wedge'}(0)\end{Bmatrix} = \begin{Bmatrix}\varphi_6^{\wedge''}(0)\\ \psi_6^{\wedge''}(0)\end{Bmatrix} = \begin{Bmatrix}\varphi_6^{\wedge'''}(0)\\ \psi_6^{\wedge'''}(0)\end{Bmatrix} = \begin{Bmatrix}0\\0\end{Bmatrix}
$$

$$
\begin{Bmatrix}\varphi_7^{\wedge}(0)\\ \psi_7^{\wedge}(0)\end{Bmatrix} = \begin{Bmatrix}0\\1\end{Bmatrix} \quad \begin{Bmatrix}\varphi_7^{\wedge'}(0)\\ \psi_7^{\wedge'}(0)\end{Bmatrix} = \begin{Bmatrix}\varphi_7^{\wedge''}(0)\\ \psi_7^{\wedge''}(0)\end{Bmatrix} = \begin{Bmatrix}\varphi_7^{\wedge'''}(0)\\ \psi_7^{\wedge'''}(0)\end{Bmatrix} = \begin{Bmatrix}0\\0\end{Bmatrix}
$$

$$
\begin{Bmatrix}\varphi_8^{\wedge}(0)\\ \psi_8^{\wedge}(0)\end{Bmatrix} = \begin{Bmatrix}0\\1\end{Bmatrix} \quad \begin{Bmatrix}\varphi_8^{\wedge'}(0)\\ \psi_8^{\wedge'}(0)\end{Bmatrix} = \begin{Bmatrix}\varphi_8^{\wedge''}(0)\\ \psi_8^{\wedge''}(0)\end{Bmatrix} = \begin{Bmatrix}\varphi_8^{\wedge'''}(0)\\ \psi_8^{\wedge'''}(0)\end{Bmatrix} = \begin{Bmatrix}0\\0\end{Bmatrix}. \tag{29}
$$

It is then possible to express the functions $f^{\wedge}(x_2)$ and $g^{\wedge}(x_2)$ as linear combinations

of the basis functions as follows:

$$\begin{Bmatrix} f^{A}(x_2) \\ g^{A}(x_2) \end{Bmatrix} = f^{A}(0)\begin{Bmatrix} \varphi_1^{A}(x_2) \\ \psi_1^{A}(x_2) \end{Bmatrix} + f^{A'}(0)\begin{Bmatrix} \varphi_2^{A}(x_2) \\ \psi_2^{A}(x_2) \end{Bmatrix} + f^{A''}(0)\begin{Bmatrix} \varphi_3^{A}(x_2) \\ \psi_3^{A}(x_2) \end{Bmatrix} + f^{A'''}(0)\begin{Bmatrix} \varphi_4^{A}(x_2) \\ \psi_4^{A}(x_2) \end{Bmatrix}$$
$$+ g^{A}(0)\begin{Bmatrix} \varphi_5^{A}(x_2) \\ \psi_5^{A}(x_2) \end{Bmatrix} + g^{A'}(0)\begin{Bmatrix} \varphi_6^{A}(x_2) \\ \psi_6^{A}(x_2) \end{Bmatrix} + g^{A''}(0)\begin{Bmatrix} \varphi_7^{A}(x_2) \\ \psi_7^{A}(x_2) \end{Bmatrix} + g^{A'''}(0)\begin{Bmatrix} \varphi_8^{A}(x_2) \\ \psi_8^{A}(x_2) \end{Bmatrix}. \quad (30)$$

Likewise, the basis function pairs $\begin{Bmatrix} \varphi_j^{B}(x_2) \\ \psi_j^{B}(x_2) \end{Bmatrix}$ $(j = 1, 2, \ldots, 8)$ can be defined in the domain $a < x_2 < b$. These functions also satisfy the governing eqns (26), as well as initial conditions which are analogous to (29), except that the initial conditions are evaluated at $x_2 = b$, instead of at $x_2 = 0$. The functions $f^{B}(x_2)$ and $g^{B}(x_2)$ can then be similarly expressed as linear combinations of the basis functions in B.

Now, it needs to be determined whether some linear combination of the basis function pairs can also satisfy the continuity conditions at $x_2 = a$. Let the velocities and traction-rates at $x_2 = a$, as evaluated in material A, be expressed in terms of $\sin \omega x_1$ and $\cos \omega x_1$ components:

$$v_1^{A}(a) = v_{1s}^{A} \sin \omega x_1 + v_{1c}^{A} \cos \omega x_1 \quad (31a)$$
$$v_2^{A}(a) = v_{2s}^{A} \sin \omega x_1 + v_{2c}^{A} \cos \omega x_1 \quad (31b)$$
$$\dot{n}_{21}^{A}(a) = \dot{n}_{21s}^{A} \sin \omega x_1 + \dot{n}_{21c}^{A} \cos \omega x_1 \quad (31c)$$
$$\dot{n}_{22,1}^{A}(a) = \dot{n}_{22,1s}^{A} \sin \omega x_1 + \dot{n}_{22,1c}^{A} \cos \omega x_1. \quad (31d)$$

Obviously, by changing the superscript A in (31) to B, analogous expressions for the velocities and traction-rates at $x_2 = a$, as evaluated in material B, are defined. Then, the interface conditions that need to be satisfied reduce to the eight equations

$$v_{1s}^{A} - v_{1s}^{B} = 0 \quad v_{1c}^{A} - v_{1c}^{B} = 0 \quad v_{2s}^{A} - v_{2s}^{B} = 0 \quad v_{2c}^{A} - v_{2c}^{B} = 0$$
$$\dot{n}_{21s}^{A} - \dot{n}_{21s}^{B} = 0 \quad \dot{n}_{21c}^{A} - \dot{n}_{21c}^{B} = 0 \quad \dot{n}_{22,1s}^{A} - \dot{n}_{22,1s}^{B} = 0 \quad \dot{n}_{22,1c}^{A} - \dot{n}_{22,1c}^{B} = 0. \quad (32)$$

To impose these conditions, one needs to express the quantities appearing in (32), in terms of the basis function pairs. This can be done by combining (13), (21), (25) and (30). It is crucial to note that the quantities in (32) depend only on the values of the basis functions and their derivatives at $x_2 = a$. Since there is no need to know anything about the basis functions except at $x_2 = a$, we can integrate the differential equations in A all the way from $x_2 = 0$ to $x_2 = a$, without extracting the solution at intermediate points; likewise, in B, we can integrate from $x_2 = b$ directly to $x_2 = a$.

Now, we introduce the numerical part of the bifurcation calculations. Instead of integrating two fourth-order ordinary differential equations to determine each of the basis function pairs and their derivatives at $x_2 = a$, we take the standard numerical route and integrate eight first-order ordinary differential equations. This necessitates the introduction of auxiliary functions which turn out to be convenient for implementing the continuity conditions. For example, in computing the basis function pair $\begin{Bmatrix} \varphi_1^{A}(x_2) \\ \psi_1^{A}(x_2) \end{Bmatrix}$, we introduce functions $y_i(x_2)$ which are defined by

$$y_1(x_2) = \varphi_1^{A}(x_2); \quad y_2(x_2) = \varphi_1^{A'}(x_2); \quad y_3(x_2) = \varphi_1^{A''}(x_2); \quad y_4(x_2) = \varphi_1^{A'''}(x_2)$$
$$y_5(x_2) = \psi_1^{A}(x_2); \quad y_6(x_2) = \psi_1^{A'}(x_2); \quad y_7(x_2) = \psi_1^{A''}(x_2); \quad y_8(x_2) = \psi_1^{A'''}(x_2). \quad (33)$$

With the initial conditions

$$y_1(0) = 1; \quad y_2(0) = y_3(0) = y_4(0) = y_5(0) = y_6(0) = y_7(0) = y_8(0) = 0 \tag{34}$$

we integrate the functions $y_j(x_2)$ from $x_2 = 0$ to $x_2 = a$. The contribution to, say, v_{1c}^{A} from the basis function pair $\begin{Bmatrix}\varphi_1^{\mathrm{A}}(x_2)\\ \psi_1^{\mathrm{A}}(x_2)\end{Bmatrix}$ can be determined using the values of y_j at $x_2 = a$, without further differentiation. Of course, this contribution is scaled by the undetermined coefficient $f^{\mathrm{A}}(0)$.

To each of the terms in (32) with a superscript A, there are eight contributions from the eight different initial conditions at $x_2 = 0$, each with its own undetermined coefficient; to each of the terms in (32) with a superscript B, there are eight contributions from the eight different initial conditions at $x_2 = b$. This results in eight equations and 16 unknowns. The remaining eight equations derive from the boundary conditions that we imposed in Section 4 on the eigenmodes. Consider, for example, the anti-symmetric mode, which corresponds to the conditions (27). In this case, the basis function pairs $\begin{Bmatrix}\varphi_j^{\mathrm{A}}(x_2)\\ \psi_j^{\mathrm{A}}(x_2)\end{Bmatrix}$ ($j = 2, 4, 6, 8$) do not contribute as their coefficient must always be zero; hence, there remain only four undetermined coefficients in A. Similarly, there are two boundary conditions at $x_2 = b$, which when applied to both the sin ωx_1 and cos ωx_1 components, reduce the number of undetermined coefficients in B to four.

All of the above boils down to setting up a system of eight homogeneous linear equations, which we represent as

$$\mathbf{Mu} = \mathbf{0} \tag{35}$$

where $\mathbf{u}$ is a vector of undetermined coefficients. Again, the first four columns of $\mathbf{M}$ (corresponding to terms with a superscript A) are arrived at by four separate integrations of the system of eight first-order ordinary differential equations in the interval $0 < x_2 < a$, each integration beginning with different initial conditions. The last four columns of $\mathbf{M}$ (corresponding to terms with a superscript B) are arrived at by similar integrations in the interval $a < x_2 < b$. The inner product of, say, the first row of $\mathbf{M}$ and the vector $\mathbf{u}$ represents continuity of v_{1c} at the interface, and likewise for the other rows. If the determinant of $\mathbf{M}$ is zero, then there exists a non-trivial vector of coefficients which satisfies all the homogeneous continuity conditions at the interface.

The numerical accuracy of this method is limited by the accuracy of the numerical integrations of the ordinary differential equations (which determine $\mathbf{M}$), and by the evaluation of the determinant of $\mathbf{M}$. With regard to the numerical integrations, we employed a highly accurate, fourth order Runge–Kutta scheme with step-size control to maintain a certain error level (Press *et al.*, 1986). In evaluating the determinant of $\mathbf{M}$, certain care must be exercised. It is convenient to express $\mathbf{M}$ in the following block form

$$\mathbf{M} = \begin{bmatrix}\mathbf{A} & \mathbf{B}\\ \mathbf{C} & \mathbf{D}\end{bmatrix} \tag{36}$$

and to use the following property of determinants

$$|\mathbf{M}| = |\mathbf{A}|\,|\mathbf{D} - \mathbf{C}\mathbf{A}^{-1}\mathbf{B}| \tag{37}$$

where $|\ |$ denotes the determinant of the enclosed matrix, and $\mathbf{A}^{-1}$ is the inverse of $\mathbf{A}$. Then, one can keep track of the subdeterminants separately, as a function of the monotonically increasing applied strain. The matrix $\mathbf{M}$ is first singular when one of the subdeterminants is first zero. As a test of the accuracy of this method, it was applied to the previously considered problem of anti-symmetric modes appearing during a homogeneous, frictionless compression (Steif, 1987). Bifurcation strains were found to be essentially identical (answers

to within seven significant figures were readily achieved), no doubt due to the accuracy control of the Runge–Kutta integrating scheme.

In a numerical search for the strain at which $|\mathbf{M}|$ first vanishes, it is crucial to break $\mathbf{M}$ into subdeterminants. The need for this is most easily appreciated when the present method is applied to the case of a homogeneous, frictionless compression. As was mentioned earlier, the $\sin \omega x_1$ and $\cos \omega x_1$ components can be considered separately (only shearing terms not present in this case cause them to be coupled); furthermore, the eigenfunctions $f(x_2)$ and $g(x_2)$ are obviously identical. The matrix $\mathbf{M}$ that is set up is such that $\mathbf{B} = \mathbf{C} = \mathbf{0}$ and $\mathbf{A} = \mathbf{D}$. While the determinant of $\mathbf{M}$ certainly vanishes when the determinant of $\mathbf{A}$ vanishes, a numerical sweep of increasing strains will not reveal a change of sign in $|\mathbf{M}|$, because $\mathbf{A}$ and $\mathbf{D}$ change sign at precisely the same strain. On the other hand, $|\mathbf{A}|$ does change signs as the point of vanishing determinant is passed. A similar problem occurs even when there is shearing and the matrix $\mathbf{M}$ is fully populated.

6. RESULTS

Bifurcation calculations were carried out in the manner described in the above sections for a variety of material parameters. A qualitative sense of the influence of shear stresses on layer bifurcation can be conveyed, however, without an exhaustive parametric study. Accordingly, the results presented here are based on computations involving a single set of material properties. We take each of the materials A and B to be described by power-law stress–strain curves of the form

$$\sigma = k\varepsilon^N$$

where k and N are constants for a given material. In particular, the material constants were chosen to be $N_A = 0.189$, $N_B = 0.367$, $k_B/k_A = 9.0$. These properties represent a symmetric stainless-steel clad aluminum. Furthermore, we assume that the thickness ratio is $a/h = 0.8333$ (each of the stainless steel layers is one-tenth as thick as the aluminum core). The central purpose of our computations is to contrast bifurcation strains for different types of prebifurcation states: (i) a homogeneous, frictionless compression (studied previously); (ii) a compression with a homogeneous shear stress; and (iii) the bimaterial Prandtl–Orowan solution. For each of states (ii) and (iii), there is a shearing parameter—γ_A/ε for (ii) and m for (iii)—which can be adjusted to vary the amount of shear relative to compression.

For state (ii), a compression with a homogeneous shear stress, we found the bifurcation strains to be negligibly different from those associated with state (i), at least for shearing ratios up to $\gamma_A/\varepsilon = 1$. Therefore, results for state (ii) are not displayed. In Fig. 6 we contrast

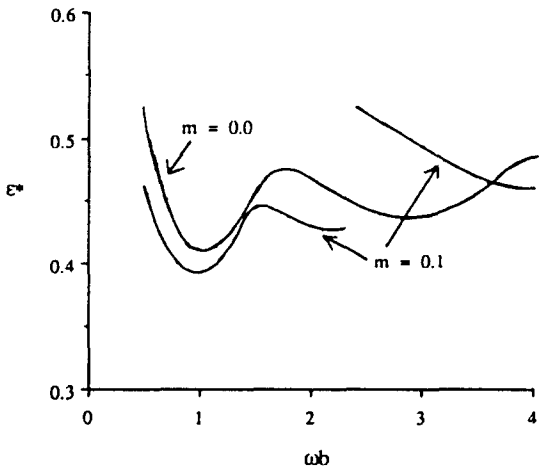

Fig. 6. Anti-symmetric mode bifurcation strain as a function of wavelength, comparing different prebifurcation states ($m = 0.0 \sim$ frictionless compression; $m = 0.1 \sim$ bimaterial Prandtl–Orowan solution).

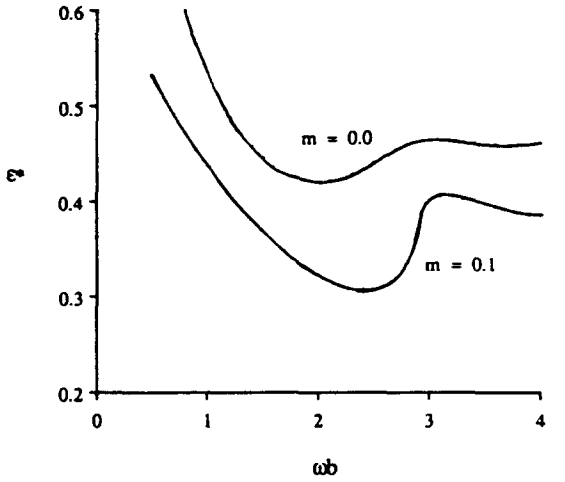

Fig. 7. Symmetric mode bifurcation strain as a function of wavelength, comparing different pre-bifurcation states ($m = 0.0 \sim$ frictionless compression; $m = 0.1 \sim$ bimaterial Prandtl–Orowan solution).

the bifurcation strains of states (i) and (iii), for the particular case of the anti-symmetric eigenmode. As explained above, $m = 0$ corresponds precisely to state (i), the homogeneous, frictionless compression. For the given set of parameters, the limiting value m^* would be roughly 0.15. It can be seen that this form of a shearing tends to diminish the bifurcation strain modestly (the difference is roughly 5%), at least in the range of wavelengths which have the lowest bifurcation strains ($\omega b \sim 1.0$). Results for the symmetric mode are shown in Fig. 7, where it can be seen that shearing *significantly* diminishes the bifurcation strain.

Variation of the anti-symmetric mode bifurcation strain with the shearing parameter m is shown in Fig. 8 for a fixed wavelength $\omega b = 1$. The modest variation can be contrasted with what is observed in the case of the symmetric mode (Fig. 9), in which the shearing has a substantial effect on the bifurcation strain. In fact, when there is substantial shearing (accounted for via the bimaterial Prandtl–Orowan solution), the symmetric mode becomes the preferred mode. This is in contrast to that which occurs in the frictionless compression, when the anti-symmetric mode emerges at a slightly lower strain.

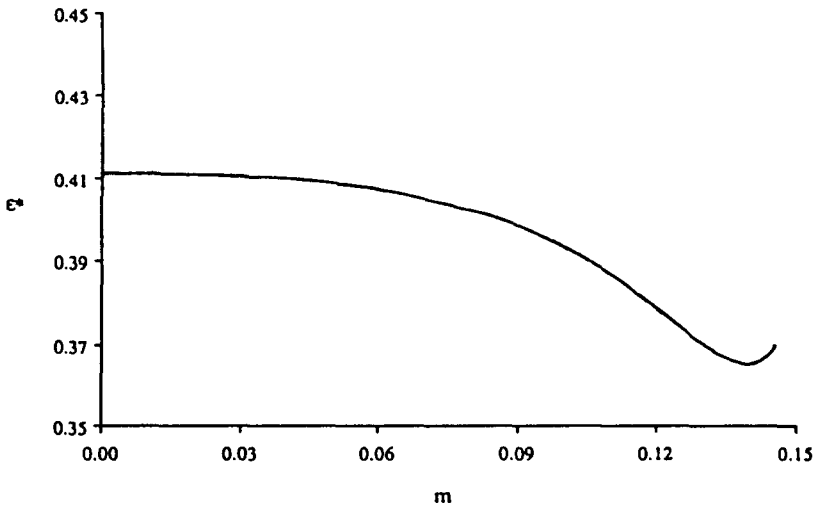

Fig. 8. Anti-symmetric mode bifurcation strain as a function of friction parameter m ($\omega b = 1.0$).

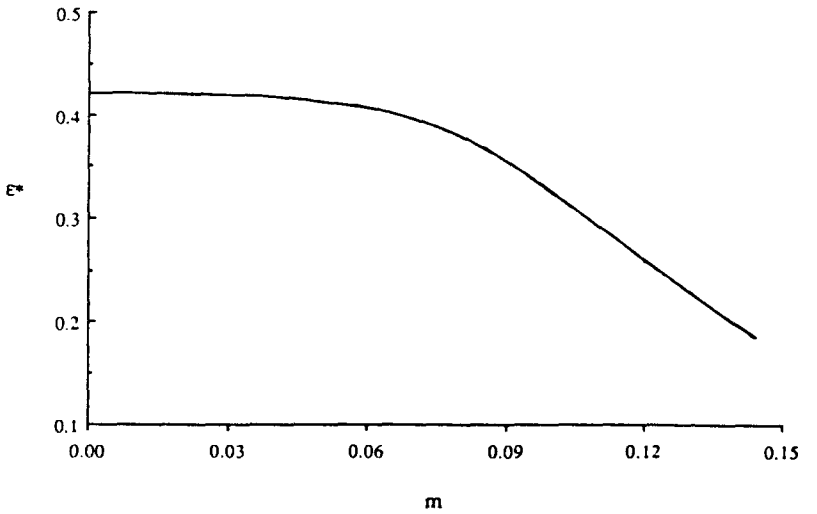

Fig. 9. Symmetric mode bifurcation strain as a function of friction parameter m ($\omega h = 2.0$).

7. SUMMARY AND CONCLUSIONS

During the rolling, or roll-bonding, of clad metals, layer thickness variations can arise which eventually led to tiger banding (periodic fracture of the cladding). A bifurcation model predicting the onset of layer thickness variations was put forth previously, in which rolling was idealized as a homogeneous, frictionless compression. The present paper has re-examined this highly idealized prebifurcation state, by employing two different prebifurcation states, each having shear stresses that are typical of rolling. Since the governing differential equation for incremental deformations essentially defies analytic solution, a suitable numerical technique was devised to obtain the bifurcation strains. A symmetrically clad, three-layered solid was considered, and the possibility of both symmetric and antisymmetric bifurcation modes (periodic layer thickness variations) was explored. We found that the presence of a homogeneous shear stress acting parallel to the layers, which could reflect rolls rotating at different speeds or an unsymmetrical layup, had a negligible effect on the predicted bifurcation strains. On the other hand, a prebifurcation state which incorporated shear stresses reflecting the friction at the rolls led to significantly lower predictions of bifurcation strains, particularly in the case of symmetric modes.

Since our bimaterial Prandtl-Orowan solution—the prebifurcation state which reflects roll friction—apparently has such a strong effect, it would be worthwhile to explore the reasonableness of this solution further. It may be recalled that this solution, while correct for a perfectly plastic solid, is approximate for a work hardening one. Perhaps a numerical solution (e.g. finite element) for the stress distribution in strain-hardening layers subjected to plane strain compression could indicate the degree of approximation in the bimaterial Prandtl–Orowan solution. In addition, it may be necessary to explore the sensitivity of our predictions to the metal–platen boundary condition. We assumed that there was zero increment in shear stress associated with the eigenmode. It is more likely, however, that the platens put up some resistance to incremental relative motion, though they do not eliminate it. Some means of incorporating this effect should be made in the future. Of course, it would be highly desirable to shed light on these issues by performing plane strain compression tests on clad metals using platens with different degrees of lubrication.

Connecting the bifurcation analysis to rolling is necessarily suspect for an additional reason. Strictly speaking, the bifurcation analysis is based on the assumption that the prebifurcation state prevails over the infinite domain $-\infty < x_1 < \infty$. One might argue that the analysis is also relevant to a finite body, provided the appropriate lineal dimension of the body, or the length in the x_1-direction over which the prebifurcation state prevails, is at least several times the wavelengths of the predicted modes. Unfortunately, the stresses of our bimaterial Prandtl-Orowan solution at best resemble the stresses induced during

rolling (as Orowan would suggest) only over some portion near the entrance to the roll gap and over some portion near the exit. Clearly, further steps are required before the bifurcation analysis can account for the very complex stress states that are associated with rolling.

Acknowledgements—Support by the National Science Foundation under grant MSM-8713806 and by the Department of Mchanical Engineering, Carnegie Mellon University is gratefully acknowledged.

REFERENCES

Hill, R. and Hutchinson, J. W. (1975). Bifurcation phenomena in the plane tension test. *J. Mech. Phys. Solids* **23**, 239–264.

Hutchinson, J. W. (1974). Plastic buckling. In *Advances in Applied Mechanics* (Edited by C.-S. Yih), Vol. 14, pp. 67–144. Academic Press, New York.

Hutchinson, J. W. and Neale, K. W. (1978). Sheet necking–II. Time-independent behavior. *Mechanics of Sheet Metal Forming*, pp. 127–153. Plenum, New York.

Karman, T. von (1925). Beitrag zur Theorie des Walzvorganges. *ZAMM* **5**, 139–141.

Orowan, E. (1943). The calculation of roll pressure in hot and cold flat rolling. *Proc. Inst. Mech. Engng* **150**, 140–167.

Prandtl, L. (1923). Anwendungsbeispiele zu einem Henckyschen Satz uber das plastische Gleichgewicht. *ZAMM* **3**, 401–406.

Press, W. H., Flannery, B. P., Teukolsky, S. A. and Vetterling, W. T. (1986). *Numerical Recipes*. Cambridge University Press, U.K.

Semiatin, S. L. and Piehler, H. R. (1979). Formability of sandwich sheet materials in plane strain compression and rolling. *Met. Trans.* **10A**, 97–107.

Steif, P. S. (1987). On deformation instabilities in clad metals subjected to rolling. *J. Appl. Metalworking* **4**, 317–326.

Steif, P. S. (1990). Interfacial instabilities in an unbonded layered solid. *Int. J. Solids Structures* **26**, 915–925.